Int J Adv Manuf Technol (2015) 78:961–969
DOI 10.1007/s00170-014-6566-0

ORIGINAL ARTICLE

The kinematics and error modelling of a novel micro-CMM

Ali Rugbani · Kristiaan Schreve

Received: 14 August 2013 / Accepted: 2 November 2014 / Published online: 23 December 2014

Abstract A novel micro-coordinate measurement machine (micro-CMM) is introduced as a viable device to be used with high precision and high accuracy measurement of part dimensions in micron scale. This design considers eliminating Abbé error, and is intended to achieve submicron accuracy for a work envelope of at least (100×100×100)mm. In this study, a prototype of the new micro-CMM was built; a mathematical measuring model to explicitly define the coordinate of the probe in x, y and z directions have been represented. An algorithm to find the workspace was implemented. The error model of the machine was created and the effect of structural errors on probe position was studied analytically. The significance of each geometric parameter was studied in order to minimize the measuring error and achieve the best machine design. Finally, the results of the analytical error model were confirmed through a Monte Carlo analysis. Moreover, the real measurements of the micro-CMM were compared with the error model.

Keywords Micro-CMM · Parallel manipulator · Micro-measurement · Covariance matrix · Error model · Monte Carlo simulation

1 Introduction

The machining, assembly inspection and quality control of small objects such as micro-electromechanical systems (MEMS) require high positioning accuracy. During the past two decades, great attention has been given to micrometrology to fill the gap between the ultrahigh precision measurements of nanometrology and macrometrology [1]. In this regard, many micro-coordinate measuring machines (micro-CMM) were introduced and intensively studied [2–4].

The fact that the errors are not cumulative and amplified is one of the major advantages of parallel CMMs over the traditional serial CMMs [5]. Nonetheless, the main disadvantage of parallel CMMs is the limited workspace [6–8] and the difficulty of their motion control due to singularity problems [5, 8]. Tian studied the assembly errors [6]. The solution of the forward kinematic for various configurations has attracted the attention of many researchers [9–16].

The performance of micro-CMMs in terms of accuracy and precision is influenced by numerous error parameters that require effective error modelling methods [17, 18]. Moreover, the error models are of great importance in order to evaluate the machine and understand the effect of the different parameters. Forward solution for error analysis was also covered [19–21].

However, The positioning accuracy of parallel mechanisms is usually limited by many errors, some authors identified the errors affecting the precision of parallel mechanisms as follows [5, 22–24]: manufacturing errors, assembly errors, errors resulting from distortion by force and heat, control system errors and actuators errors, calibration and even errors due to mathematical models. These errors should be divided into two main sources, static errors for those not dependent on the dynamics and process forces, and dynamic errors for errors due to the movement and measuring method [25].

1.1 Dynamic errors

These types of errors are dependent on the configuration of the machine. Dynamic errors occur only during operating the machine and depend on the velocity, the acceleration and the forces applied on the end effector. The main sources are friction, wear and backlash occurring in the joints and actuators and deflection in the legs. Additionally, elastic deformations of the machine kinematics through process forces or

A. Rugbani (✉) · K. Schreve
Department of Mechanical and Mechatronic Engineering, Stellenbosch University, Stellenbosch, South Africa
e-mail: rugbani@gmail.com

inertial forces and natural vibrations of the machine can be other sources of dynamic errors.

1.2 Static errors

A high static accuracy is a basic requirement for any micromeasuring machine. Obviously, the actual geometry of any machine does not match exactly its design. These differences may cause small positional changes of the probe. The machine then must be properly calibrated to identify its geometric parameters. Any manufacturing and assembly errors of the machine components, especially the joints, will introduce kinematic errors [26]. Sensor errors are caused by angular errors of the actuator (Abbé's effect) and bending load caused by the weight of the actuator itself [27].

Abbé error is a major source of error in precision measurements. The magnitude of angular error due to the effect of Abbé error is dependent on the pitch and yaw angles on the measuring axis and the offset from the measured object. Abbé error is determined by multiplying the angle in radians by the offset (Abbé error = angle × offset). McCarthy, in [28], claimed that the Abbé error is roughly equal to 5 nm per 1 mm of offset and arc second of angular error.

The kinematic errors can be drastically reduced by proper manufacturing and assembly of the machine parts and sensors. Previous studies showed the influence of joint manufacturing and assembly on the positioning error [5, 17]. Moreover, Huang et al. [29] studied the assembly errors and used manual adjustable mechanisms to control assembly errors. The elastic deformations of the machine structure due to the flexibility of machine components could lead to gravitational errors; a numerical control unit can be used to compensation for the gravitation errors [30]. Moreover, thermal errors should be considered as another source that significantly affects the accuracy due to the thermal deformations and expansion of the legs [30]. Thermal errors can be reduced by compensating for the resulting thermal deformation of the components using a very complex thermal model [30]. Tsai [31], Raghavan [32] and Abderrahim and Whittaker [33] have studied the limitations of various modelling methods.

Static errors are claimed to have the most significant effect on the machine accuracy [30]. Nevertheless, in high-precision micro-CMMs, the positional error of dynamic sources must be considered. Pierre [34] showed that the operation and the performance of the sensors significantly affect the precision of the manipulator. Hassan analysed the tolerance of the joints [35].

This paper presents a micro-CMM based on parallel mechanism [36, 37]. Its workspace was analysed, and details of the measuring model are reported. An error model of the mechanism given the law of error propagation using covariance matrix theory was established, and the effect of geometrical errors on the position were analysed.

2 Machine design and structure

The micro-CMM designed in this research consists of a moving tetrahedron frame with fixed angles between its legs, its main vertex pointing downwards. The legs of this frame are carried by three runner blocks where they can slide freely. The runner blocks are connected to the actuated prismatic joints with spherical joints. Moreover, laser distance sensors are installed on the edges of the moving frame in order to acquire accurate measurement of the length of the legs. The movement of the prismatic joints are controlled by three linear motors. 3D view and top view of the machine are shown in Fig. 1, and a schematic drawing of the micro-CMM machine is showing in Fig. 2.

The arrangement of this micro-CMM provide movement in 3 ° of freedom (3-DOF), translation in z direction, rotation around x-axis and rotation around y-axis. In other 3-DOF manipulators, like Oiwa's design [36], the workspace is very small because of the limitation of using rotational joints. This arrangement provides significant advantage by using spherical joints. The use of spherical joints ensures that larger workspace is achieved. Any point within the workspace can be reached by controlling the vertical position of the three linear actuators. This design is also singularity free within the whole workspace, which is beneficial to the

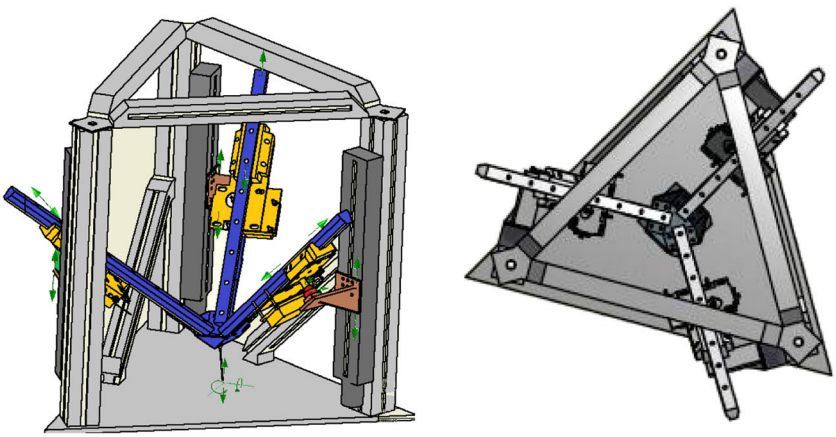

Fig. 1 Micro-CMM design. 3D (*left*) and top view (*right*)

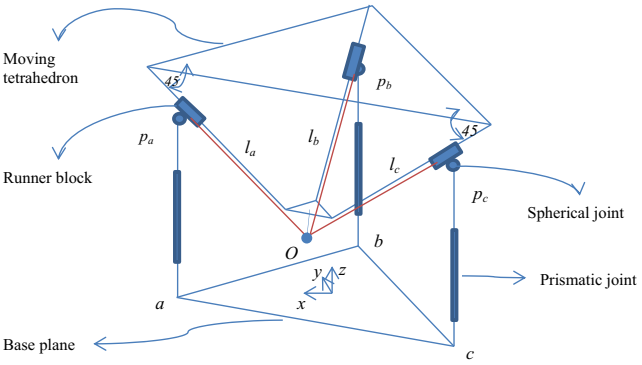

Fig. 2 Schematic drawing of the micro-CMM machine

motion control. Error due to joints is minimized because of the reduced number of joints and connections, compared to other conventional parallel manipulators. The design considers theoretically eliminating Abbé error since the laser distance sensors are located in the axes of movement and always pointing towards the probe tip, where the resulting offset is virtually avoided. Figure 2 shows a schematic drawing of the micro-CMM machine.

3 Coordinate system

The coordinate system is shown in Fig. 3. The origin $O(0, 0, 0)$ is placed at the centre of the base. The prismatic joints intersect with the base at points a, b and c; x-axis equally divides the angle at point a and the z-axis is perpendicular to the base plane (a, b, c).

The geometrical parameters are as follows:

l_i is the distance between pivot point of the ball joint p_i and the probe tip p_o

$l_{\min}$ and $l_{\max}$ are the maximum and minimum extensions of the legs, $l_{\min}=300$ mm, $l_{\max}=550$ mm

θ_i is the angle between the tetrahedron legs l_i, l_{in}; $\theta_a=\theta_b=\theta_c=68$ °

4 Development of the kinematic model

Assume that the probe tip (x, y, z) is at the main vertex of the moving tetrahedron, which is the point of intersecting of the three legs. Because of spherical joints, the equation of movement of the legs can be expressed by the following governing equations:

$$l_a^2 = (x-x_a)^2 + (y-y_a)^2 + (z-z_a)^2 \quad (1)$$

$$l_b^2 = (x-x_b)^2 + (y-y_b)^2 + (z-z_b)^2 \quad (2)$$

$$l_c^2 = (x-x_c)^2 + (y-y_c)^2 + (z-z_c)^2 \quad (3)$$

From Fig. 4, it is clear that values of the z coordinate of the moving motors (z_{i+1} and z_{i-1}) can be calculated relative to the z component of the stationary motor (z_i), where distances $dz_{i,i+1}$ and $dz_{i-1,i}$ can be calculated provided that the legs l_a, l_b and l_c, as well as angels (β) between them are known.

Let the subscript i and represent (a, b, c) when i rotates around z-axes in clockwise direction when seen from above, subscripts ip and in refer to the previous and next points, respectively.

$$z_{in} = z_i - dz_{in}; z_{ip} = dz_{ip} - z_i \quad (4)$$

$$dz_{in}^2 = (d_{in})^2 - (b_{in})^2; \quad dz_{ip}^2 = (d_{ip})^2 - (b_{ip})^2 \quad (5)$$

$$d_{in}^2 = l_i^2 + l_{in}^2 - 2\, l_i l_{in} \cos(\beta_{in}); \quad d_{ip}^2 = l_{ip}^2 + l_i^2 - 2\, l_{ip} l_i \cos(\beta_{ip}) \quad (6)$$

Where:

i is the pivot point of the i^{th} joint, $i=[a, b, c]$

in and ip are the pivot point of the next and previous pivot points, respectively

dz is the height difference between the pivot point of the joint on stationary motor and moving joints

d_{in} and d_{ip} are the distance between i^{th} pivot point and the next and previous pivots, respectively

b_{in} and b_{ip} are the distance between p_1 and p_2 at $z_2=z_1$ and $z_3=z_1$, respectively

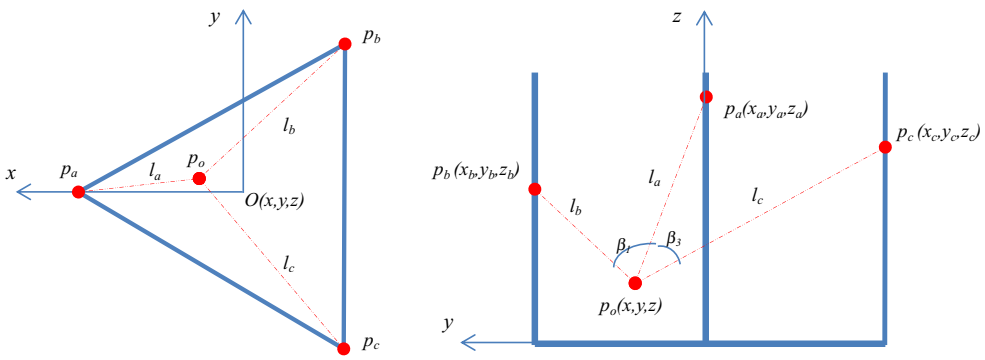

Fig. 3 The coordinate system: top view xy plane (*left*), and front view yz plane (*right*)

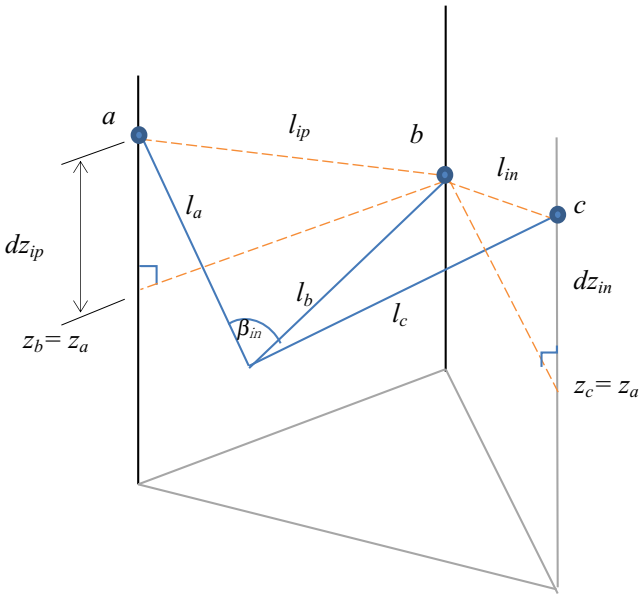

Fig. 4 Schematic drawing of the micro-CMM machine. Point b is stationary, points a and c are moving

β_{in} and β_{ip} is the angles between leg l_i and legs l_{in} and l_{ip}, respectively

At the start of the operation, z is assumed to be equal to zero, or alternatively, the stationary point will have $z=-z_i$, and $z_i=0$.

The coordinate of the probe location can be found by solving Eqs. (1), (2) and (3). and replacing the values of z_{in} and z_{ip} from Eq. (4). This yields explicit expressions for the x, y and z coordinates of the centre point of the probe as follows:

$$y = \frac{-v \pm \sqrt{v^2 - 4uw}}{2u} \tag{7}$$

$$z = F + D\,y \tag{8}$$

$$x = A + B\,y \tag{9}$$

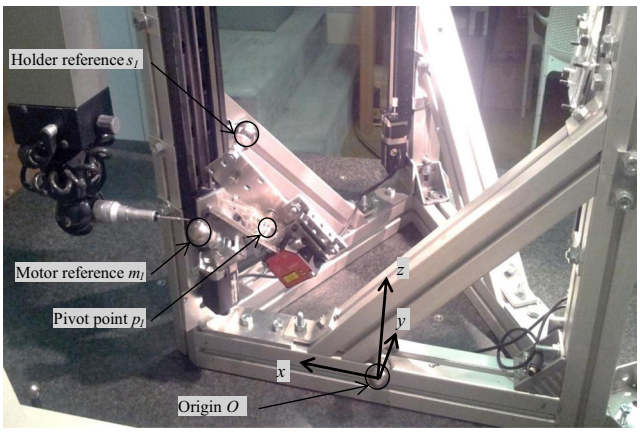

Fig. 5 Photograph of the machine

Where:

$$A = \frac{\left(\frac{c_{in}-c_i}{2\,z_{in}} - \frac{c_i-c_{ip}}{2\,z_{ip}}\right)}{\left(\frac{x_i-x_{ip}}{z_{ip}} - \frac{x_{in}-x_i}{z_{in}}\right)}; \qquad B = \frac{\left(\frac{y_i-y_{in}}{z_{ip}} - \frac{y_{ip}-y_i}{z_{in}}\right)}{\left(\frac{x_i-x_{ip}}{z_{ip}} - \frac{x_{in}-x_i}{z_{in}}\right)};$$

$$D = \frac{y_{in}-y_i}{z_{in}} - B\frac{x_{in}-x_i}{z_{in}}; \quad F = A\frac{x_{in}-x_i}{z_{in}} - \frac{c_{in}-c_i}{2\,z_{in}}; \quad c_i = l_i^2 - x_i^2 - y_i^2 - z_i^2$$

$$u = 1 + B^2 + D^2$$

$$v = 2DF + 2x_iB - 2AB + 2y_i$$

$$w = A^2 + F^2 - 2\,x_iA - c_i$$

5 Modelling of the kinematic error

5.1 Analytical error model

Suggesting an error model for the proposed machine is of great importance in order to evaluate the structure and understand the effect of the different parameters on its accuracy. This method uses first-order Tylor approximation and assumes uncorrelated input noise. The derivation of the covariance matrix is well known and can be found in refs. [38–40]. The covariance matrix (Λ_F) can be written as:

$$\Lambda_F = J\left(\bar{x}\right)\,\Lambda_x\,\mathrm{J}\left(\bar{x}\right)^T \tag{10}$$

where: $J(x)$ is the Jacobian matrix of $F(x)$ and $\bar{x}$ is the average of all x samples.

The last equation is very useful to determine the covariance matrix using the input covariance and the Jacobian of the process function.

In this study, the error of each stage (or leg) is a combination of errors in the leg length l_i and the position of the spherical joint p_i in the Cartesian coordinate system.

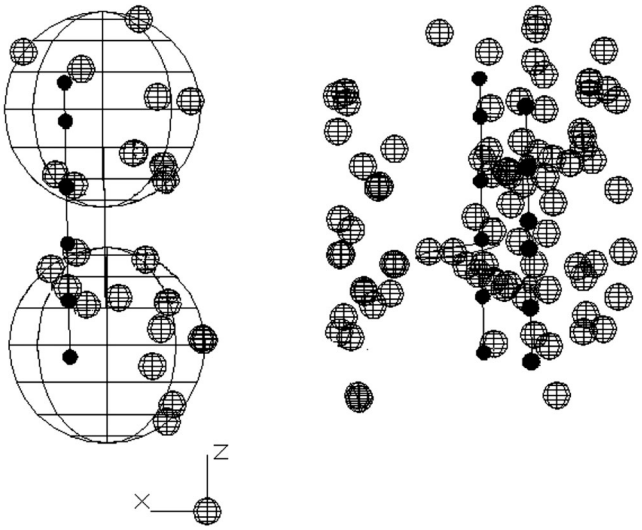

Fig. 6 Shows the measurements taken by means of CMM

These measurement errors are created mainly by the error in the spherical joints es_i, parallelism in the runner blocks eb_i, backlash in the motors em_i, capability of the laser distance sensor ed_i, angular errors of the actuator, cosine error *ecos* and Abbé error eab_i. Elastic deformations and deflection of the moving structure is represented by the small change in the angle between the legs of the tetrahedron $e\theta_i$. Probe error *ep* and effects of thermal expansions are considered minimal and were not included in the error model.

Therefore, a total of 15 parameters will be investigated. A full-size Jacobian matrix is used in carrying out error analysis, the Jacobian consists of the first-order partial derivatives of *x, y* and *z* in Eqs. (7), (8) and (9) with respect to the error sources. The Jacobian needed is organized in a 3×15 matrix, as follows:

$$J = \begin{bmatrix} \frac{\partial x}{\partial x_a} & \frac{\partial x}{\partial x_b} & \frac{\partial x}{\partial x_c} & \frac{\partial x}{\partial y_a} & \frac{\partial x}{\partial y_b} & \frac{\partial x}{\partial y_c} & \frac{\partial x}{\partial z_a} & \frac{\partial x}{\partial z_b} & \frac{\partial x}{\partial z_c} & \frac{\partial x}{\partial l_a} & \frac{\partial x}{\partial l_b} & \frac{\partial x}{\partial l_c} & \frac{\partial x}{\partial ecos} & \frac{\partial x}{\partial eab} & \frac{\partial x}{\partial \theta} \\ \frac{\partial y}{\partial x_a} & \frac{\partial y}{\partial x_b} & \frac{\partial y}{\partial x_c} & \frac{\partial y}{\partial y_a} & \frac{\partial y}{\partial y_b} & \frac{\partial y}{\partial y_c} & \frac{\partial y}{\partial z_a} & \frac{\partial y}{\partial z_b} & \frac{\partial y}{\partial z_c} & \frac{\partial y}{\partial l_a} & \frac{\partial y}{\partial l_b} & \frac{\partial y}{\partial l_c} & \frac{\partial y}{\partial ecos} & \frac{\partial y}{\partial eab} & \frac{\partial y}{\partial \theta} \\ \frac{\partial z}{\partial x_a} & \frac{\partial z}{\partial x_b} & \frac{\partial z}{\partial x_c} & \frac{\partial z}{\partial y_a} & \frac{\partial z}{\partial y_b} & \frac{\partial z}{\partial y_c} & \frac{\partial z}{\partial z_a} & \frac{\partial z}{\partial z_b} & \frac{\partial z}{\partial z_c} & \frac{\partial z}{\partial l_a} & \frac{\partial z}{\partial l_b} & \frac{\partial z}{\partial l_c} & \frac{\partial z}{\partial ecos} & \frac{\partial z}{\partial eab} & \frac{\partial z}{\partial \theta} \end{bmatrix} \quad (11)$$

The related variances matrix is given by the following 15× 15 diagonal matrix:

$$\Lambda_p = \begin{bmatrix} \sigma_{x_a}^2 & 0 & \cdots & 0 \\ 0 & \sigma_{x_b}^2 & & \\ \vdots & & \ddots & \\ 0 & 0 & \cdots & \sigma_\theta^2 \end{bmatrix} \quad (12)$$

In the previous matrix, the variance along the diagonal is given for, x_a, x_b, x_c, y_a, y_b, y_c, z_a, z_b, z_c, l_a, l_b, l_c.*ecos, eab, eθ*. Precision error values are mostly considered as three times the standard deviation value ($\varepsilon=3\sigma$). Thus, the variance can be estimated by:

$$\sigma_p{}^2 = \left(\frac{\varepsilon_p}{3}\right)^2 \quad (13)$$

where $\sigma_p{}^2$ and ε_p are the variance and the error of the parameters, respectively.

5.2 Parameter identification and calibration

Calibration of this novel micro-CMM was performed by the means of a conventional Mitutoyo CMM Bright Apex 710, which is available at the metrology laboratory of the University of Stellenbosch; the CMM has a volumetric accuracy of 5 μm according to the latest calibrated.

5.3 Coordinate setup

Before starting with the calibration process of the micro-CMM, a permanent coordinate system was introduced. This coordinate system is important for any future calibration or parameter identification. Reference standard ball (*O*) was used to represent the origin, ball *O* is attached to the middle of the lower horizontal frame connecting points *a* and *b*, *xz* plane is perpendicular to the base plane and *xy* is parallel to the base.

5.4 Geometry of the machine structure

The spherical joints are connected by brackets to the linear actuated motors, this gives a translational movement in the vertical direction. The linear path of movement is identified by the following technique: reference ball (m_i) is attached to each bracket of the three motors. The master CMM is used to measure m_i at six different positions along the horizontal path of the moving motors. At each position, the spherical joints' pivot point p_i were calculated using another standard ball (*s*); ball s_i is attached to the runner block. The centre of s_i was

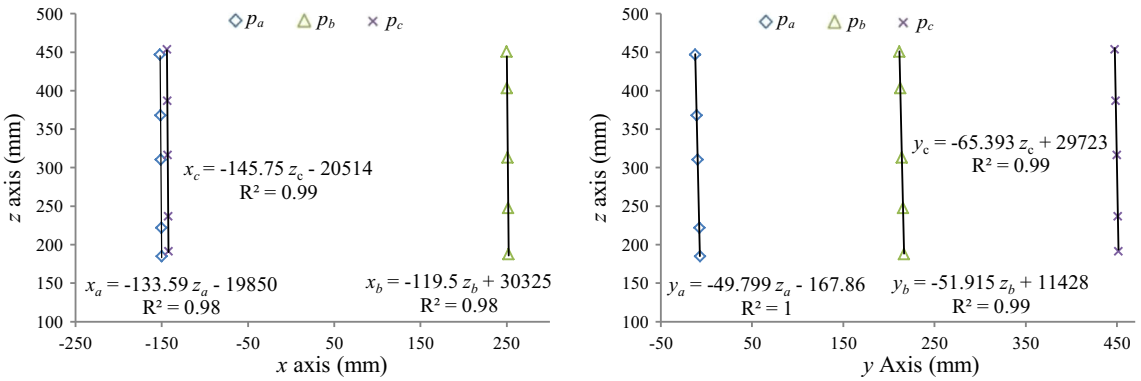

Fig. 7 Calculation of points p_i, *xz* plane (*left*) and *yz* plane (*right*)

measured on at least eight different positions; the centre of a sphere fitting of points s_i's represent point p_i.

In order to define the vertical movement of the linear motors, pivot points p_i were calculated at six different vertical positions of point m_i. Figure 5 shows a photograph of the structure showing balls m_i, p_i, s_i and O, as well as the master CMM that is used to determine their positions.

Consider the fact that the distance m_i–p_i is supposed to be always fixed; therefore, position of point p_i can be determined with respect to the position of point m_i. The CAD drawing for these measurements is displayed in Fig. 6.

In Fig. 6, centre of the solid black spheres represent point m_i, small spheres represent ball s_i, and centre of the largest spheres represent point p_i. The figure shows the measurements of m_i at six vertical positions, and for clarity sphere fitting and measurements taken for s_i are shown at only two positions of m_i, namely position nos. 1 and 5. Figure 7 shows front view (right) and side view (left) of the machine, the figure demonstrate the path of movement of the three pivots of the spherical joints: points p_a, p_b and p_c. Each vertical path of movement of p_i at (a, b and c) was represented by five different vertical positions. The coordinate components of x and y are calculated as a function of z component.

Error in p_i was estimated as the difference between the measurements taken by the master CMM and the calculated values using equations given in Fig. 7. Standard deviations of differences in x direction for points a, b and c are (0.015, 0.035, 0.010)mm, respectively. And in y direction are (0.013, 0.016, 0.041)mm, respectively

5.5 Geometry identification of the tetrahedron

In this step, the geometrical parameters of the tetrahedron were measured; angle between the legs and distance between the leg outer surface and the probe tip, were measured. Figure 8 shows the tetrahedron taking measurements using the master CMM.

5.6 Dead distance

The total length of the leg l_i is the total distance between the spherical joint pivot point p_i and the probe tip p_o. l_i is the sum of the following distances:

l_i is the (distance between p_i and laser source + distance between the reflective surface and p_o) + laser reading

$$l_i = d_i + r_i$$

where d_i is the dead distance and r_i is the laser reading

The length d_i can be found if the positions p_i and p_o are known; where p_i is calculated using reference point m_i, and p_o is measured using the master CMM by measuring the centre

Fig. 8 Parameter identification of the moving part, fixed tetrahedron

of the ball tip of the micro-CMM's probe, as shown in Fig. 9, then the inverse kinematics of the machine is solved to identify the length of the leg l_i. The dead distance d_i can then be calculated.

For this step, the length was calculated at 10 positions and d_i was determined. Dead distance for the legs were found to be d_a=294.047 mm, d_b=289.906 mm and d_c=289.402 mm. With the following standard deviations: σ_a=0.107 mm, σ_b= 0.126 mm and σ_c=0.113 mm.

5.7 Abbé error

The most important angular error affecting linear positioning accuracy is the result of Abbé error. Abbé effect decreases as the distance between the axes of measurement and the probe tip decreases, this distance is known as offset. Since the laser distance sensor is located in the axes of movement and pointing towards the probe tip, the resulting offset is virtually avoided.

Fig. 9 Photograph of the parameter identification process

Table 1 Error sources on the micro-CMM

Error	Source	Affects	Design values	Actual values
es_i	Machining limitation	x_i, y_i, z_i	1 μm	1.5 μm
eb_i	Machining limitation	x_i, y_i	Nanometer	40 μm
ed_i	Manufacturing limitation	l_i	1 nm	50 μm
em_i	Backlash	z_i	Nanometer	1 μm
ecos	Assembly	*x*, *y*, *z*	0	NA
eabbe	Design/assembly	*x*, *y*, *z*	Angle 0.05 arc second offset 10 μm	48 nm
ep	Manufacturing limitation	*x*, *y*, *z*	0.08 μm	0.5 μm
$e\beta_i$	Geometry	z_{in}, z_{ip}	0	70 μm

Suppose that the arrangement can produce an estimated angle of 50 arc seconds, and the offset of the laser distance sensor is not more than 0.2 mm. Then, Abbé error can be approximated as 0.2 mm×tan (50 arc seconds)=48 nm.

Table 1 lists the design values of the expected errors and the actual values resulting from the devices and hardware used in this machine.

Best possible configuration can be achieved as per the information provided in Table 1 in order to reach the ultimate goal of submicron accuracies, by attending to the following recommendations: improving the rigidity of the structure to reduce the dynamic errors resulting from the effect of vibration and the weight of the moving parts. Adding triple beam laser interferometer to replace the existing optoNCDT 1302 laser distance sensor from micro-epsilon, virtual elimination of Abbé error is achieved by using a triple beam laser interferometer, which is capable to measures pitch and yaw angles with 0.02 arc second angular resolution. Moreover, reducing the legs' length and mounting the encoder at minimum possible dimensional offset between the probe tip and the measuring axes would be effective. Using of super precision class spherical rolling joints run-out less than 1 μm compared to the existing 2 μm for the standard precision class SRJ joints. Runner blocks can be replaced by sliding contact bearings to achieve nano meter accuracy as proposed by Smith and Robbie [41]. Moreover, operating in a temperature-controlled environment minimizes the thermal effect.

6 Results

The micro-CMM is characterized to confirm the validity of the proposed kinematic model and the analytical error model. The measurements of the micro-CMM are compared to the measurements done with the master CMM. Thirty points were measured; the positions of these measured points in *xy* plane are illustrated in Fig. 10. 3D view of the points is given in Fig. 11.

The analytical error model (AM) is used to confirm that the error in the measurements falls within the error budget

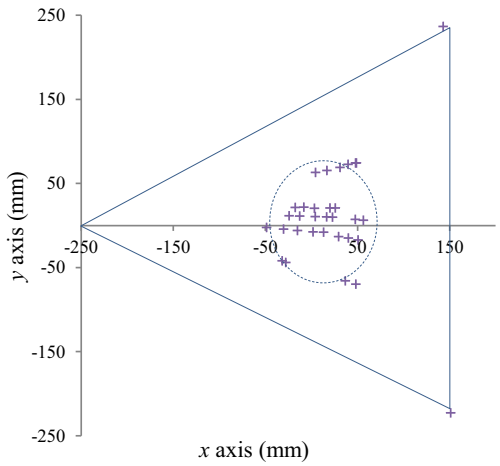

Fig. 10 Measured points and the workspace of the micro-CMM

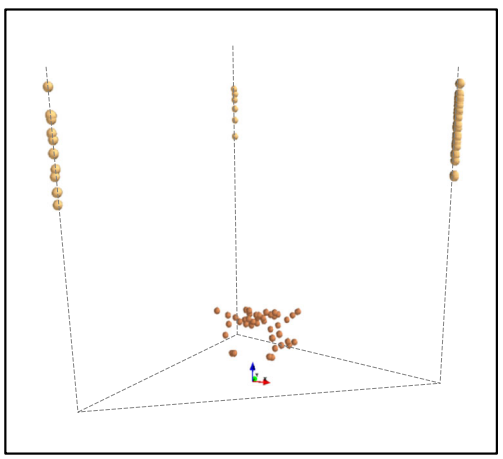

Fig. 11 Measured points using micro-CMM

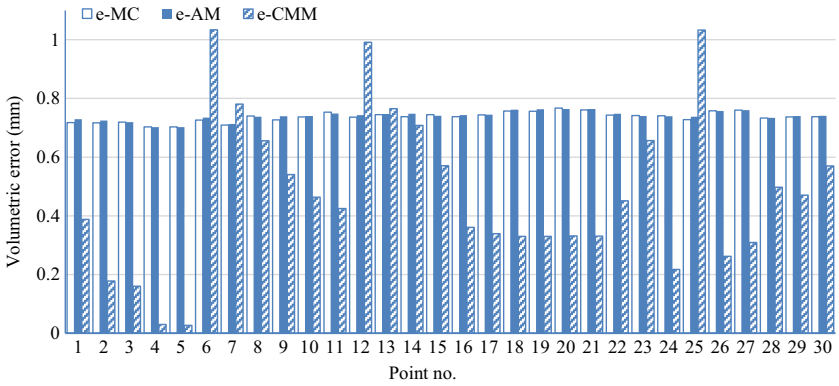

Fig. 12 error comparison; micro-CMM vs. AM vs. MC

estimated by the error model. Monte Carlo simulation (MC) is also included in the comparison to confirm the validity of the results. Monte Carlo simulation uses random values of the error sources, and the standard deviation of the results (σ) is calculated for 10,000 iterations.

A comparison of the error in the CMM reading with the expected error, estimated as 3.σ, by MC and AM, respectively, in 30 different positions is given by Fig. 12. In the figure, the error comparison is given by three bars for each point. Hatched bars represent the error values between the micro-CMM readings and the measured CMM (ecmm), solid bars represent the estimated error using AM, and the unfilled bars represent the expected error using MC simulation. In the figure, all the results are presented as a volumetric error value, estimated as 3σ by MC, and 3 $\sqrt{\sigma^2}$ by AM.

From Fig. 12, it is clear that for most of the measured points, the error falls within an acceptable range of the error budget estimated by the simulation and analytically. Even though the graph shows some points that have outliers such as on point numbers 6, 12 and 25, these errors are due to the difference between the micro-CMM and the CMM used for the calibration, which may be attributed to the effect of a lot of external factors, such as human error in taking measurements or mechanical vibration.

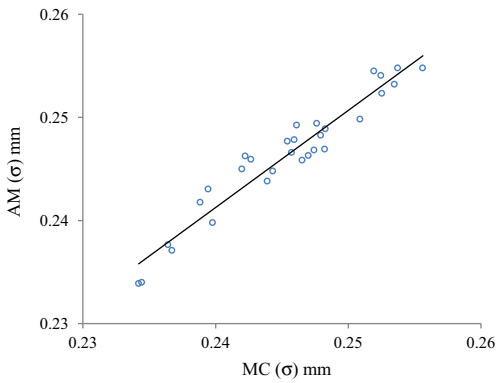

Fig. 13 Analytical AM versus simulation MC comparison

The results of the analytical error model AM match very well with the simulation results MC on all points. The standard deviation results of AM and MC increases and decreases in the same trend as shown in Fig. 13.

Previous results show that the proposed analytical error model is valid and can be used as a robust tool for an error estimation model for the micro-CMM machine under study. The best possible configuration of the micro-CMM can be achieved as per the design values listed in Table 1. The same error model is still valid to estimate the error values for the machine. The results show that the machine can achieve sub micron accuracy with standard deviation of (x=70 nm, y=60 nm, z=50 nm).

7 Conclusion

In this paper, a new micro-CMM was designed and the first prototype of the machine was built; the kinematic model, as well as the error model, was derived. Calibration of the new micro machine was done by the means of coordinate measuring machine.

It can be observed from the results that the kinematic problem can be solved using the proposed direct kinematic model. Moreover, the practical experiments confirmed that the analytical error model is effective in estimating the error budget for the machine; this was verified using Monte Carlo simulation results.

Submicron measurements are achievable with this concept, provided that the design values listed in Table 1 are implemented.

Operating in a temperature-controlled environment, error compensation and good calibration models will definitely reflect on improved accuracy.

References

1. McKeown P (1998) Nanotechnology-special article. in *Nano-metrology in precision engineering*, Hong Kong. pp. 5–55
2. Gao F, Lin W, Zhao X (2002) New kinematic structures for 2-, 3-, 4-, and 5-DOF parallel manipulator designs. Mech Mach Theory 37: 1395–1411
3. Kuang-Chao F, Yetai F, and Xiaofen Y (2005) Development of a micro-CMM in *International manufacturing leaders forum on "global competitive manufacturing"*. Adelaide, Australia pp 1–7
4. Liu X, Wang J, Pritschow G (2005) A new family of spatial 3-DOF fully-parallel manipulators with high rotational capability. Mech Mach Theory 40:475–494
5. Gang C, Ge S, Wang Y (2007) Error analysis of three degree-of-freedom changeable parallel measuring mechanism. J China Univ Min Technol 17(1):101–104
6. Hunt K (1983) Structural kinematics of in parallel-actuated robot arms. ASME J Mech Transm Autom Des 105:705–712
7. Clavel R and Delta, (1988) A fast robot with parallel geometry in *International symposium on industrial robots*, Switzerland. pp 91–100
8. Craig J (1989) Introduction to robotics: mechanics and control, 2nd edn. Addison and Wesley, New York
9. Dhingra A, Almadi A, Kohli D (2000) Closed-form displacement analysis of 8, 9 and 10-link mechanisms. Mech Mach Theory 35: 821–850
10. Xiaolun S and Fenton R, (1994) "A complete and general solution to the forward kinematics problem of platform-type robotic manipulators," *IEEE*, pp 3055–3062
11. Didrit O, Petitot M, Walter E (1998) Guaranteed solution of direct kinematic problems for general configurations of parallel manipulators. IEEE Trans Robot Autom 14(2):259–266
12. Zhang, Chang-de and Shin-Min S (1991) Forward kinematics of a class of parallel (Stewart) platform with closed-form solutions in *IEEE international conference on robotics and automation*, Sacramento, California, pp 2676–2681
13. Nanua P, Waldron K, Murthy V (1990) Direct kinematic solution of a Stewart platform. IEEE Trans Robot Autom 6(4):431–437
14. Sreenivasan S, Waldron K, Nanua P (1994) Closed-form direct displacement analysis of a 6–6 Stewart platform. Mech Mach Theory 29(6):855–864
15. Griffis M, Duffy J (1989) A forward displacement analysis of a class of Stewart platform. J Robot Syst 6(6):703–720
16. Lin W, Griffis M, Duffy J (1992) Forward displacement analyses of the 4–4 Stewart platforms. Trans ASME 114:444–450
17. Yao R, Tang X, Li T (2010) Error analysis and distribution of 6-SPS and 6-PSS reconfigurable. Tsinghua Sci Technol 15(5):547–554
18. Lin C, Tang X, Wang L (2007) Precision design of modular parallel kinematic machines. Tool Eng 41(8):38–42
19. Jian W and Oren M (1993) On the accuracy of a Stewart platform—Part I: The effect of manufacturing tolerances in *IEEE international conference on robotics and automation Los Alamitos*. Atlanta, GA, USA, pp. 114–120
20. Chunhe G, Jingxia Y, Jun N (2000) Nongeometric error identification and compensation for robotic system by inverse calibration. Int J Mach Tools Manuf 40:2119–2137
21. Patel A, Ehmann K (2000) Calibration of a hexapod machine tool using a redundant leg. Int J Mach Tools Manuf 40:489–512
22. Meng C (2004) Error model and error compensation of six-freedom-degree parallel mechanism CMM. J Harbin Inst Technol 36(3):317–320
23. Li M, Weibin R, Lining S, and Zheng L (2006) Error compensation for a parallel robot using back propagation neural networks in *International conference on robotics and biomimetics*. Kunming, pp. 1658–1663
24. Meng M, Che R, Huang Q, Yu Z (2002) The direct-error-compensation method of measuring the error of a six-freedom-degree parallel mechanism CMM. J Mater Process Technol 129: 574–578
25. Pritschow G, Eppler C, and Garber T (2002) Influence of the dynamic stiffness on the accuracy of PKM," in *3rd Chemnitz parallel kinematics seminar*. Chemnitz, pp 313–333
26. Soons J (1998) On the geometric and termal errors of a hexapod machine tools in *The first European-American forum on parallel kinematic machines*. Milano, pp 151–170
27. Weck M and Staimer D (2002) Accuracy issues of parallel kinematic machine tools *Proceedings of the Institution of Mechanical Engineers, Part K: Journal of Multi-body Dynamics*. vol. 216, no. K, pp. 51–58, M Weck and D Staimer
28. McCarthy K (1991) Accuracy in positioning systems in *The motion control technology*. pp 19–21
29. Huang T, Li Y, Tang G, Li S, Zhao X, Whitehouse D, Chetewyn D, Liu X (2002) Error modeling, sensitivity analysis and assembly process of a 3-DOF parallel mechanism. Sci China (Ser E) 45(5): 628–635
30. Pandilov Z, Dukovski V (2010) Survey of the dominant error types at parallel kinematics machine tools. Int J Eng 8(1):193–196
31. Tsai L (1999) Robot analysis—the mechanics of serial and parallel manipulators. Wiley, New York
32. Raghavan M (1993) The Stewart platform of general geometry has 40 configurations. ASME J Mech Des 115:277–282
33. Abderrahim M, Whittaker A (2000) Kinematic model identification of industrial manipulators. J Robot Comput Integr 16:1–8
34. Pierre R, Nicolas A, and Philippe M (2005) Kinematic calibration of parallel mechanisms: a novel approach using legs observation *IEEE transactions on robotics*. vol. 4, pp. 529–538
35. Mahir H, Leila N (2005) Design modification of parallel manipulators for optimum fault tolerance to joint jam. Mech Mach Theory 40: 559–577
36. Oiwa T (1997) New coordinate measuring machine featuring a parallel mechanism. Int J Jpn Soc Precis Eng 31(3):232–233
37. Zhuang H and Wang Y, (1997) A coordinate measuring machine with parallel mechanisms in *IEEE Int. ConJ: on robotics and automation*, Albuquerque, New Mexico, pp 3256–3261
38. Rugbani A and Schreve K, (2012) Modelling and analysis of the geometrical errors of a parallel manipulator micro-CMM in *6th international precision assembly seminar IPAS2012*, Chamonix France, pp 105–117
39. Zhao Z and Perey F (1992) The covariance matrix of derived quantities and their combination, Oak Ridge National Laboratory. Beijing, China, Technical report ORNL/TM-12106
40. Clarke J (1998) Modelling uncertainty: a primer, Department of Engineering, Oxford University, Oxford, UK, Technical report
41. S Smith and C Robbi, Subnanometer surface texture and profile measurement with 'Nanosurf 2'. *Annals of the CIRP*, vol. 37, no. 1, pp. 519–522, 1988